http://dx.doi.org/10.5012/bkcs.2014.35.4.1191

First Simultaneous Visualization of SO_2 and NO_2 Plume Dispersions using Imaging Differential Optical Absorption Spectroscopy

Hanlim Lee, Youngmin Noh,[†] Soonchul Kwon,[‡] Hyunkee Hong, and Kyung-Soo Han[*]

Department of Spatial Information Engineering, Pukyong National University, Busan 608-737, Korea
[*]E-mail: kyung-soo.han@pknu.ac.kr
[†]Department of Environmental Science and Engineering, Gwangju Institute of Science and Technology, Gwangju 500-712, Korea
[‡]School of Civil and Environmental Engineering, Georgia Institute of Technology, Atlanta, GA 30332, USA
Received December 21, 2013, Accepted January 4 2014

Imaging Differential Optical Absorption Spectroscopy (Imaging-DOAS) has been utilized in recent years to provide slant column density (SCD) distributions of several trace gas species in the plume. The present study introduces a new method using Imaging-DOAS data to determine two-dimensional plume structure from the plume emissions of power plant in conditions of negligible aerosol effects on radiative transfer within the plume. We demonstrates for the first time that two-dimensional distributions of sulfur dioxide (SO_2) and nitrogen dioxide (NO_2) in power plant emissions can be determined simultaneously in terms of SCD distribution. The SO_2 SCD values generally decreased with increasing distance from the stack and with distance from the center of the plume. Meanwhile, high NO_2 SCD was observed at locations several hundred meters away from the first stack due to the ratio change of NO to NO_2 in NOx concentration, attributed to the NO oxidation by O_3. The results of this study show the capability of the Imaging-DOAS technique as a tool to estimate plume dimensions in power plant emissions.

Key Words : Plume dimension, Plume dispersion, Imaging-DOAS, Nitrogen dioxide, Sulfur dioxide

Introduction

Sulfur dioxide (SO_2) and nitrogen oxide (NO_x = NO + NO_2) are both known to play important roles in local and global atmospheric chemistry. A large proportion of the sulfur as sulfur dioxide induces aerosol formation and acid deposition as it is quickly oxidized in the atmosphere after being emitted in fossil fuel combustion, resulting in deleterious effects on human health.[1] In Addition, NO_x is associated with the surface-level catalytic formation of ozone and is known to have adverse effects on vegetation and human health.[2] Among the various anthropogenic activities involving fossil fuel combustion, power plant operation is a major contributor as an emission source to global anthropogenic emissions, which releases these two trace gases.

Many studies have analyzed NO_x and SO_2 plume emissions from power plant stacks in an effort to clarify their chemical and physical characteristics either at the emission source, the stack outlet, or at ground sites in some distance from the stack using conventional trace gas measurements at the source using in-situ instruments.[3-6] Several types of remote sensing techniques are available for observing the temporal and spatial characteristics of these gases in plume emitted from various point sources such as power plants and volcanoes, such as Correlation SPECtrometer (COSPEC) method,[7] the SO_2 camera technique,[8] Fourier-Transform spectroscopy in the IR (FT-IR),[9-11] and passive differential optical absorption spectroscopy (DOAS). However, these methods do not support simultaneous measurements of multiple trace gases.

For this reason, we carried out the techniques using Multi-Axis Differential Optical Absorption Spectroscopy[12] and Imaging-DOAS[13] to investigate plume dimensions and the spatial characteristics of multiple trace gases for their simultaneous observation.[14-20] During observation, passive DOAS techniques directly measure the slant column density (SCD) of the absorber that is the integral of the absorber concentration present over the path between a light source and the detector. The spatial distribution of SCD over the plume area provides information about the plume dimensions and reveals the distribution of absorbers in a single direction.

Using the passive Imaging-DOAS technique, this study introduced the characteristics of two-dimensional SO_2 and NO_2 distributions, measured simultaneously in terms of SCD in power plant emissions for the first time. Detailed studies on the characterization and the potential application of Imaging-DOAS measurements for remote sensing of spatial distributions are described in this investigation.

Experimental

Field Measurement and Instrument Description. The Imaging-DOAS technique measures the two-dimensional (2D) spatial distribution of ambient trace gases using scattered sunlight as a source of radiation that has passed through a 2D area of interest, measured via sequential scanning of the vertical columns comprising the target using a horizontally rotating mirror.

Figure 1(a) illustrates the horizontal and vertical measurement geometries with the locations of the first (westernmost)

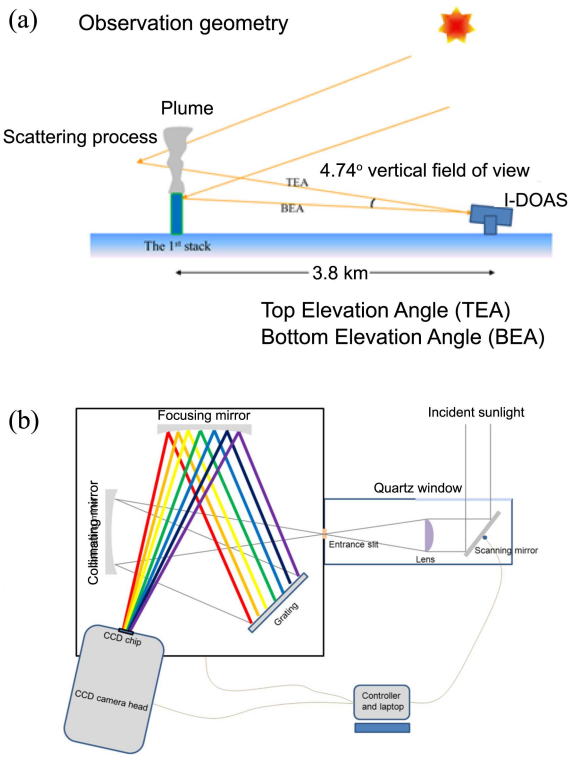

Figure 1. (a) Observation geometry of the Imaging-DOAS instrument. (b) Schematic description of the Imaging-DOAS instrument seen from the top.

and last (easternmost) stacks, respectively. The Imaging-DOAS measurements, located in near TaeAn power plant stacks, were carried out at a remote site (36.54°N, 126.14°E) located off the west coast of Korea for three measurement days (October 14, 15, and 17, 2008). The Imaging-DOAS instrument consists of entrance optics composed of a quartz lens (Plano convex, f = 100 mm) and a scanning mirror, and a spectrometer attached with a 2D charge-coupled device (CCD) detector (Figure 1(b)). The mirror reflects the scattered sunlight onto a convex lens. The lens focuses the reflected light onto the entrance slit of the spectrometer (Spectro2DA; Czerny Turner type, f/# 3.9, Spectro Inc., Gwangju, Korea), which disperses the light through a grate. The light is then focused onto a 2D CCD chip (Symphony; 26.6 × 6.9 mm in size; 2048 × 512 pixels, Horiba JobinYvon Inc., Edison, USA) on the camera head. The single pixel size scanned by the instrument is 14.3 m (h) × 3.9 m (v) at the target location. In order to reduce CCD exposure time and the cross-talk effect between vertical pixels caused by the finite point spread function (PSF),[13] the vertically resolved 512 CCD rows were binned into groups of 8, yielding 64 rows for the vertical spatial pixels during the measurement period. The vertical field-of-view toward the target was 4.74° with a resolution of 0.06°.

Analysis of Spectra. The recorded Imaging-DOAS data were analyzed to derive SO_2 and NO_2 SCDs using WinDOAS software[21] and the DOAS analysis method.[22] After each measurement, the CCD noise (including dark current and offset signals) was subtracted from each measured spectra. Spectra acquired from a direction opposite to the wind direction were used as Fraunhofer reference spectra (FRS). Dividing each FRS by the respective spectrum recorded at the same binned rows of the CCD chip allowed the removal of Fraunhofer features and elimination of background SO_2 and NO_2 absorption signals in the measured spectra. A hyper-spectral solar spectrum was fitted to the FRS to retrieve wavelength information.[23] The absorption cross-sections of SO_2,[24] NO_2,[25] ozone (O_3) at temperatures of 243 and 293 K,[26] and O_4 [27] were convoluted with individual slit functions, determined for each binned row of the CCD chip. NO_2 and O3 were Io-corrected using WinDOAS software. Ring spectra were calculated from the individual FRS using DOASIS software.[28,29] To retrieve SO_2 SCDs, the convoluted SO_2, NO_2, O_3, the Ring spectra, and a 3rd order polynomial that accounts for slowly varying absorption characteristics due to aerosol and air molecules were simultaneously fitted to the measured optical densities, which is obtained from the logarithm of each FRS divided by the respective spectrum over the wavelength interval between 312 and 321 nm encompassing the three SO_2 absorption bands. In order to retrieve NO_2 SCDs, the convoluted NO_2, O_4, the Ring spectra, and a 3rd order polynomial were fitted to the measured optical densities at a different wavelength interval between 379 and 393 nm containing five NO_2 absorption bands.

Results and Discussion

Spatial Distributions of SO_2 and NO_2 SCDs. The leftmost (westernmost) stack is hereafter referred to as the 'first' stack and the rightmost (easternmost) is referred to as the 'last' stack. The plume from these stacks was invisible in actual measurement, implying a negligible water vapor plume from the stack emission compared to those with a visible plume, but SO_2 and NO_2 emissions are shown simultaneously in Figures 2-4. With regard to stack location, the first stack exit location is easily recognized in Figure 4(a), as explained later in this section.

Figures 2(a) and 2(b) show the distributions of SO_2 and NO_2 SCDs, respectively, measured by the Imaging-DOAS instrument from 10:30–10:39 on October 14, and Figures 3(a) and 3(b) show those measured from 14:20–14:31 on October 15. The spatial distributions of the SO_2 SCDs clearly differ from those of NO_2 SCDs in both figures. In Figure

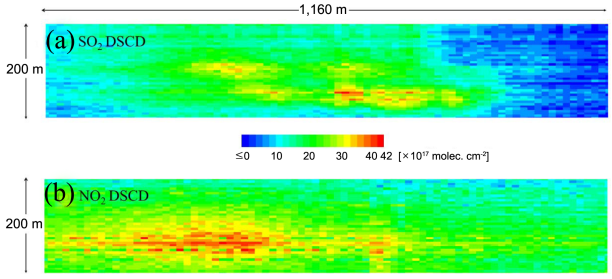

Figure 2. (a) SO_2 and (b) NO_2 SCD distributions derived from the Imaging-DOAS spectra taken between 10:30 and 10:39 on October 14.

2, SO_2 SCD values generally exhibited a decreasing pattern from the stack exits and center locations of the SO_2 plume to the plume edges. The high SO_2 SCD values observed near the stack exits can be attributed to high SO_2 mixing ratios while that observed at the center locations of the plume image could be due to a long path length taken within the plume. Given that the northeasterly wind was dominant over the measurement site during this measurement period, the plume drifted towards the southwest from the stack location. Thus, light path length along the line-of-sight of the instrument is considered to contribute largely to the measured SCDs. SO_2 SCD values were as high as 3.6×10^{18} molec cm^{-2} in the fresh plume emission and as low as 8.0×10^{15} molec cm^{-2}, which likely corresponded to the background SO_2 level. This background SO_2 level was observed on the right-hand side of the image, which is not thought to be directly affected by the fresh plume emission. In contrast, most of the scanned areas were covered with high NO_2 SCDs, as shown in Figure 2(b). This difference between SO_2 and NO_2 SCD distributions could be significantly affected by the chemical reactions of NO with O_3 because most NO_x is emitted in the form of NO. Additionally, NO usually oxides with O_3 much faster than SO_2 in heterogeneous reactions since O_3 is one of the most available oxidants. It is worth noting that SO_2 does not undergo chemical reactions in close proximity to the stack exits whereas the ratio of NO to NO_2 in NO_x concentration can change with downwind distance from the stacks.

The distributions of SO_2 and NO_2 shown in Figure 3 are similar to, but slightly different from those shown in Figure 2. Because the high SO_2 SCDs were observed near the stacks, the gases shown at the bottom of the image and the SO_2 plume likely rose up and simultaneously moved toward the instrument, which was located southward from the stacks because the northerly wind was dominant at that time. Interestingly, the distributions of enhanced SO_2 were similar to those of NO_2 with high SCDs near the stacks and on the right side of the plume images, suggesting that plume propagation was directed toward the instrument or in a completely opposite direction, in which case the light path lengthened significantly within the plume along the line-of-sight. Otherwise, the SO_2 and NO_2 distributions differed although high NO_2 SCDs are distributed over a much larger area compared to SO_2.

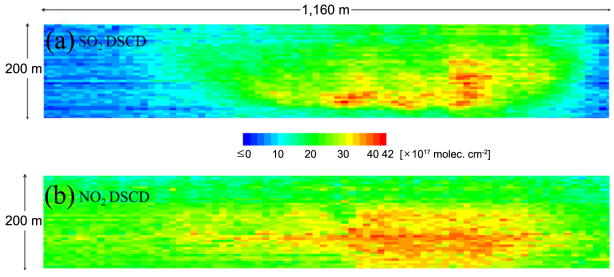

Figure 3. (a) SO_2 and (b) NO_2 SCD distributions derived from the Imaging-DOAS spectra taken between 14:20 and 14:31 on October 15.

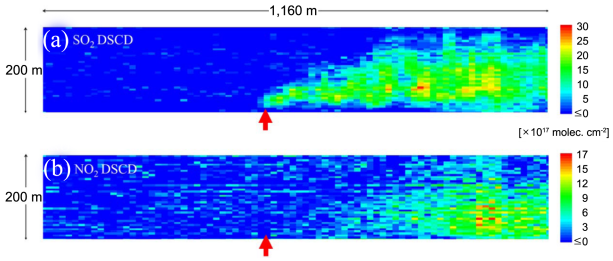

Figure 4. (a) SO_2 and (b) NO_2 SCD distributions derived from the Imaging-DOAS spectra taken between 10:05 and 10:17 on October 17. The red arrow indicates the location of the first stack exit.

Figures 4(a) and 4(b) show the distribution of SO_2 and NO_2 SCDs, respectively, measured by the Imaging-DOAS instrument from 10:05–10:17 on October 17 when a westerly wind was dominant. As mentioned previously, the location of the first stack exit, which is the starting point of the leftmost and bottommost pixel of the SO_2 plume, is easily distinguished in Figure 4(a). According to the SO_2 SCD distribution, the plume appears to have propagated from the first stack to the last stack and toward the right-hand side of the observed SO_2 image area, following the wind direction. Enhanced SO_2 SCDs were observed at the center of the plume image while values decreased from the center to the edge of the plume. NO_2 was not observed at the first stack exit location, but high NO_2 SCD values were observed at some distance downwind from the first stack. This was likely the result of the time needed for the oxidation of NO to NO_2.

Conclusion

This study developed a new way to estimate the two-dimensional distributions of the SO_2, NO_2 plume simultaneously, according to their slant column density (SCD) distributions. The SO_2 SCD gradually decreased with an increase in distance from the power plant stack. On the other hand, the high NO_2 SCD was still observed at the locations of several hundred meters away from the emission stack. It is found that the ratio of NO to NO_2 in NO_x concentration has been changed with downwind distance from the stacks due to the oxidation of NO by ozone (O_3), leading to the continuous observation of NO_2 SCD. The findings of this study demonstrate the potential capability of Imaging-DOAS measurements not only for remote sensing of spatial distributions of atmospheric trace gases, but also for estimating the two-dimensional distribution of the plume, which is useful for improving and validating plume dispersion models. To improve the results obtained using this application, further efforts need to focus on the three-dimensional distribution of the plume and the distributions of SO_2 and NO_2 mixing ratio.

Acknowledgments. This work was supported by a National Research Foundation of Korea (NRF) grant funded by the Korea government (MEST) (No. 2012R1A1A2004834). The software package WinDOAS used to evaluate Imaging-

DOAS spectra was provided by the Belgium Institute for Space Aeronomy, Belgium.

References

1. Katsouyanni, K.; Touloumi, G.; Spix, C.; Schwartz, J.; Balducci, F.; Medina, S.; Rossi, G.; Wojtyniak, B.; Sunyer, J.; Bacharova, L.; Schouten, J. P.; Ponka, A.; Anderson, H. R. *British Med. J.* **1997**, *314*, 1658-1663.
2. Agency, U. E. P. National Air Quality and Emissions Trends Report 1997; Research Triangle Park, N.C., 1998.
3. Hewitt, C. N. *Atmos. Environ.* **2001**, *35*, 1155-1170.
4. Luria, M.; Imhoff, R. E.; Valente, R. J.; Tanner, R. L. *Atmos. Environ.* **2003**, *37*, 3593-3603.
5. Luria, M.; Valente, R. J.; Tanner, R. L.; Gillani, N. V.; Imho, R. E.; Mueller, S. F.; Olszyna, K. J.; Meagher, J. F. *Atmos. Environ.* **1999**, *33*, 3023-3036.
6. Springston, S. R.; Kleinman, L. I.; Brechtel, F.; Lee, Y.; Nunnermacker, L. J.; Wang, J. *Atmos. Environ.* **2005**, *39*, 3431-3443.
7. Sandsten, J.; Edner, H.; Svanberg, S. *Opt. Lett.* **1996**, *21*, 1945-1947.
8. Mori, T.; Burton, M. *Geophy. Res. Lett.* **2006**, *33*, L24804.
9. Harig, R.; Matz, G.; Rusch, P. *Instrumentation for Air Pollution and Global Atmospheric Monitoring* **2001**, *4574*, 83-94.
10. Love, S. P.; Goff, F.; Schmidt, S. C.; Counce, D.; Pettit, D.; Christenson, B. W.; Siebe, C. *Geophy. Mono.* **2000**, *116*, 117-138.
11. Verma, S. K.; Deb, M. K.; Verma, D. *Atmos. Res.* **2008**, *90*, 33-40.
12. Hönninger, G.; von Friedeburg, C.; Platt, U. *Atmos. Chem. Phys.* **2004**, *4*, 231-254.
13. Lohberger, F.; Honninger, G.; Platt, U. *Appl. Opt.* **2004**, *43*, 4711-4717.
14. Bobrowski, N.; Honninger, G.; Galle, B.; Platt, U. *Nature* **2003**, *423*, 273-276.
15. Bobrowski, N.; Honninger, G.; Lohberger, F.; Platt, U. J. *Volcano. Geoth. Res.* **2006**, *150*, 329-338.
16. Bobrowski, N.; von Glasow, R.; Aiuppa, A.; Inguaggiato, S.; Louban, I.; Ibrahim, O. W.; Platt, U. *J. Geophy. Res.* **2007**, *112*, D06311.
17. Heue, K. P.; Wagner, T.; Broccardo, S. P.; Walter, D.; Piketh, S. J.; Ross, K. E.; Beirle, S.; Platt, U. *Atmos. Chem. Phys.* **2008**, *8*, 6707-6717.
18. Lee, H.; Kim, Y. J.; Jung, J.; Lee, C.; Heue, K. P.; Platt, U.; Hu, M.; Zhu, T. *J. Environ. Manage.* **2009**, *90*, 1814-1823.
19. Louban, I.; Bobrowski, N.; Rouwet, D.; Inguaggiato, S.; Platt, U. *Bull. Volcano.* **2009**, *71*, 753-765.
20. Pikelnaya, O.; Flynn, J. H.; Tsai, C. *J. Geophy. Res.* **2013**, *118*, 8716-8728.
21. Van Roozendael, M.; Fayt, C. *WinDOAS 2.1 Software User Manual*, Uccle, IASB/BIRA, 2001.
22. Platt, U.; Stutz, S. *Verlag Berlin Heidelberg*, 2008.
23. Kurucz, R. L.; Furenlid, I.; Brault, J.; Testerman, L. *Solar Flux Atlas from 296 nm to1300 nm (National Solar Observatory Atlas, No. 1)*; New Mexico: 1984.
24. Vandaele, A. C.; Simon, P. C.; Guilmot, J. M.; Carleer, M.; Colin, R. *J. Geophy. Res.* **1994**, *99*, 25599-25605.
25. Voigt, S.; Orphal, J.; Burrows, J. P. *J. Photoch. Photobio. C* **2002**, *149*, 1-7.
26. Bogumil, K.; Orphal, J.; Homann, T.; Voigt, S.; Spietz, P.; Fleischmann, O. C.; Vogel, A.; Hartmann, M.; Kromminga, H.; Bovensmann, H.; Frerick, J.; Burrows, J. P. *J. Photochemistry and Photobiology A* **2003**, *157*, 167-184.
27. Herman, C.; Vandaele, A. C.; Carleer, M.; Fally, S.; Colin, R.; Jenouvrier, A.; Coquart, B.; Mérienne, M. F. *Environ. Sci. Pollu. Res.* **1999**, *6*, 151-158.
28. Fish, D. J.; Jones, R. L. *Geophy. Res. Lett.* **1995**, *22*, 811-814.
29. Kraus, S., DOASIS–A Framework Design for DOAS. Aachen, 2006.